Металлофиз. новейшие технол. / Metallofiz. Noveishie Tekhnol.
2014, т. 36, № 5, сс. 597–611
Оттиски доступны непосредственно от издателя
Фотокопирование разрешено только
в соответствии с лицензией

СТРОЕНИЕ И СВОЙСТВА НАНОРАЗМЕРНЫХ И МЕЗОСКОПИЧЕСКИХ МАТЕРИАЛОВ

PACS numbers: 68.35.Dv, 79.60.Bm, 82.65.+r, 82.80.Pv, 82.80.Rt

XPS/ToF-SIMS Characterization of TiO_2 Supported Au Nanoparticles: Effect of Catalytic CO Oxidation

S. P. Chenakin, N. Kruse*, M. A. Vasylyev, and I. N. Makeeva

G. V. Kurdyumov Institute for Metal Physics, N.A.S. of Ukraine,
36 Academician Vernadsky Blvd.,
UA-03680 Kyyiv-142, Ukraine
**Université Libre de Bruxelles, Chimie-Physique des Matériaux,*
CP 243,
1050 Bruxelles, Belgium

X-ray photoelectron spectroscopy (XPS) and time-of-flight secondary ion mass spectrometry (ToF-SIMS) are employed for a comparative study of the surface composition and electronic structure of an Au/TiO_2 catalyst in the as-prepared state and after using it in the reaction of CO oxidation at room temperature. As found, the reaction-induced changes in the morphology of Au nanoparticles related to their agglomeration are accompanied by modification of the electronic state of the catalyst via an enhanced electron transfer to the gold atoms that shows up as an additional negative shift of the Au 4*f* spectrum and its distortion. The catalytic reaction of CO oxidation results in the loss of hydroxyl groups and accumulation on the support surface of various carbon-containing species with the leading formation of carbonate and bicarbonate groups, which increases with time on stream. The role of these factors in deactivation of the catalyst is discussed.

За допомогою рентґенівської фотоелектронної спектроскопії (РФЕС) та часопролітної вторинно-іонної мас-спектрометрії (ЧП-ВІМС) проведено порівняльне дослідження складу поверхні й електронної структури каталізатора Au/TiO_2 у свіжоприготованому стані та після його використання у реакції окиснення CO за кімнатної температури. Встановлено, що індуковані каталітичною реакцією зміни у морфології наночастинок Au, які спричинені їхньою аґломерацією, супроводжувалися модифікуванням електронного стану каталізатора завдяки посиленому перенесенню електронів на атоми золота, що проявлялося як додатковий неґативний зсув РФЕ-спектра Au 4*f* і його спотворення. Каталітична реакція окиснення CO призводила до втрати гідроксильних груп та накопичення на поверхні підкладки різних вуглецевмісних функціональних груп з переважним

формуванням карбонатів і бікарбонатів, яке посилювалося з часом реакції. Обговорюється роль цих чинників у деактивації каталізатора.

С помощью рентгеновской фотоэлектронной спектроскопии (РФЭС) и времяпролётной вторично-ионной масс-спектрометрии (ВП-ВИМС) проведено сравнительное исследование состава поверхности и электронной структуры катализатора Au/TiO_2 в свежеприготовленном состоянии и после его использования в реакции окисления CO при комнатной температуре. Установлено, что индуцированные каталитической реакцией изменения в морфологии наночастиц Au, вызванные их агломерацией, сопровождались модификацией электронного состояния катализатора путём усиленного переноса электронов на атомы золота, что проявлялось в виде дополнительного отрицательного сдвига РФЭ-спектра Au 4*f* и его искажения. Каталитическая реакция окисления CO приводила к потере гидроксильных групп и накоплению на поверхности подложки различных углеродсодержащих функциональных групп с преимущественным формированием карбонатов и бикарбонатов, которое усиливалось с течением времени реакции. Обсуждается роль этих факторов в деактивации катализатора.

Key words: Au/TiO_2 catalyst, carbonates, CO oxidation, sintering, XPS, ToF-SIMS.

(Received 25 December, 2013)

1. INTRODUCTION

Gold nanoclusters supported on various metal oxides have been extensively studied, since they exhibit high catalytic activity for various types of reactions of industrial interest. In particular, performance of the most active titania-supported gold catalysts, Au/TiO_2, in low-temperature CO oxidation has received considerable attention that stems from a variety of potential practical applications [1]. Numerous experimental methods have been applied in the search for the active site in the CO oxidation over supported gold catalysts, in determining the influence of various parameters on the surface composition and physicochemical state of the catalysts. In particular, X-ray photoelectron spectroscopy (XPS) has been widely used, mainly because changes in the chemical and electronic state of small metal clusters can be routinely monitored, using this technique.

Appreciation of the chemical and physical changes that can occur during catalytic reaction is very important for understanding the performance of catalysts and the causes of their deactivation. In this regard, *in situ* XPS can especially be helpful due to its potential to identify mechanistically essential transient species under reaction conditions [2]. On the other hand, post-reaction *ex situ* XPS characterization of Au catalysts, or analysis of the 'quenched' states, proved to be

useful for ascertaining the reaction effect on the oxidation state and electronic structure of gold nanoparticles. Park and Lee [3] were probably the first who compared the Au 4*f* XP spectra of calcined Au/Fe_2O_3 and Au/Al_2O_3 catalysts before and after reaction of CO oxidation at 313 K performed under the dry and wet conditions. As was established, during the reaction in the dry condition the oxidized gold phases (Au_2O_3 in Au/Fe_2O_3, $Au(OH)_3$ and Au_2O_3 in Au/Al_2O_3), which coexisted in the as-prepared catalysts along with Au^0, were reduced almost completely to metallic Au, however after the reaction in the wet condition about 40% of the oxidic gold remained. The gradual reduction of Au^{III} species to metallic gold in an Au/Fe_2O_3 catalyst was also observed in work [4], whereas in an Au/CeO_2 catalyst the Au^{III} ions were reduced under CO oxidation reaction conditions to Au^+ species [5].

The data on the chemical and electronic state of gold nanoparticles in different catalysts used in the CO oxidation as determined by the Au 4*f* binding energy are rather contradictory, although they clearly indicate that formation and modification of the particles' electronic state strongly depend on the nature of support. For the Au/TiO_2 system, in which gold was in a metallic state, the reaction of CO oxidation was observed to cause an appreciable shift of the Au^0 4*f* peak to lower binding energies as compared to the fresh catalyst [6, 7]. A similar negative shift of the Au 4*f* and Au 4*d* lines was also reported for an Au/Al_2O_3 catalyst used in the CO oxidation [8]. Conversely, in works [7, 9] no significant shift of the Au 4*f* line was detected for Au/Al_2O_3 and Au/TiO_2 catalysts after CO oxidation. Also, the position of the Au 4*f* line was noted to remain practically unaffected in the used Au/ZrO_2 [7, 10] and Au/MnO_x [11] catalysts.

The aim of the present work was to systematically study the influence of reaction of CO oxidation at room temperature on the surface composition, chemical state and electronic structure of two Au/TiO_2 catalysts prepared by using different routes and, accordingly, to revisit the reported Au 4*f* core-level shifts. For this purpose, we employed XPS and time-of-flight secondary ion mass spectrometry (ToF-SIMS) which are known to be most suitable analytical techniques for characterization of physical-chemical state of the surface of materials and provide valuable complementary information.

2. EXPERIMENTAL

The Au/TiO_2 catalyst was prepared by deposition–precipitation (DP) technique. In the first series, titania was obtained by precipitation of titanium oxalate $Ti(C_2O_4)_2$ from titanium tetraisopropoxide $Ti(OC(CH_3)_3)_4$ using a 1.5-fold excess of oxalic acid dihydrate in acetone. The dried precipitate was subsequently decomposed under (O_2 + + 10% Ar) ambient at 525°C during 4 h to form TiO_2. XRD confirmed

titania to be present as anatase. Deposition–precipitation of Au on the as-prepared TiO_2 support occurred from an aqueous solution of $HAuCl_4$, the precipitating agent being urea H_2NCONH_2. The precipitate was subsequently subjected to temperature-programmed oxidation (3°C/min, 10% O_2 in Ar) followed by calcination at 300°C for 2 h. We denote this sample 'DP1'.

In the second series, the Au/TiO_2 catalyst 'DP2' was prepared in the same way as DP1 but the oxalate route to TiO_2 was modified, namely, to test the possible catalytic influence of Mg, precipitation of $Ti(C_2O_4)_2$ was performed at a reduced oxalic acid excess but with adding $MgNO_3{\cdot}6H_2O$ to the solution in the amount which should provide doping of TiO_2 with 0.04% wt. Mg. In both catalysts, DP1 and DP2, the resulting Au loading was about 1.5% wt. According to TEM measurements, the average diameter of Au nanoparticles was 3.0–3.9 nm. The Brunauer–Emmet–Teller (BET) surface area of the Au/TiO_2 catalysts was $\cong$100 m^2/g. Note that the catalysts DP1 and DP2 were prepared in a sodium-free environment.

Catalytic CO oxidation tests over Au/TiO_2 catalysts were performed at room temperature in a 2% CO + 2% O_2 (Ar balance) gas mixture, with the flux being 50–100 ml/min. The duration of catalytic reaction test was 60 min for DP1 and 151 min for DP2.

The surface physicochemical state of the catalysts was studied in a combined XPS/ToF-SIMS instrument at a base pressure of $5.2{\cdot}10^{-10}$ mbar. For XPS, a non-monochromatic MgK_α-radiation was used at an operating power of 15 kV×10 mA. Prior to analysis, the samples were outgassed for 100 h in a preparation chamber at a base pressure of $6{\cdot}10^{-10}$ mbar. Photoelectron core-level spectra were acquired with a hemispherical analyzer in the constant-pass-energy mode at $E_p = 50$ eV with a 0.05 eV energy step. The overall resolution of the spectrometer in this operating mode was 0.96 eV. Au 4*f* core-level spectra recorded from a pure sputter-cleaned Au foil were used as a reference for bulk metallic gold, and the spectrometer was calibrated against the Au $4f_{7/2}$ line set at 84.0 eV. To minimize X-ray damage of the catalyst [12], acquisition of core-level spectra was started immediately after exposing the sample to the operating X-ray source and the exposure was kept as low as possible. After subtraction of the Shirley-type background, the core-level spectra were decomposed into their components with mixed Gaussian–Lorentzian lines by a non-linear least squares curve-fitting procedure, using a public software package XPSPEAK 4.1. Deconvoluted peak areas and standard sensitivity factors [13] were used to evaluate the surface composition of the samples. The carbon C 1*s* line at 284.8 eV was taken as a reference for surface-charging corrections.

Static ToF-SIMS analysis of the catalyst was carried out with a pulsing (7.7 kHz) beam of 5 keV Ar^+ ions, using a reflection analyzer. Positive secondary ions were registered in the mass range up to $m/z = 400$

with a mass resolution of $m/\Delta m = 1230$ at 51 a.m.u.

XPS-SIMS measurements were carried out for the as-prepared calcined Au/TiO_2 catalyst (hereinafter referred to as 'Fresh') and for the same catalyst after its using in reaction of CO oxidation (denoted 'Used'). Both samples, the fresh and the used catalyst, were loaded on the sample holder and analyzed sequentially, under the same experimental conditions. The measurements were performed for two samples of each catalyst (DP1 and DP2) and the data were reproducible.

3. RESULTS AND DISCUSSION

The sample DP1 demonstrated the highest catalytic activity and good stability during the time of the test, with the CO to CO_2 conversion being about 88%. The catalytic activity of DP2 was somewhat lower but also rather stable; with increasing reaction time up to 151 min the CO to CO_2 conversion gradually decreased from 81 to 79% (Fig. 1).

Figure 2 shows characteristic XPS core-level spectra for an Au/TiO_2 catalyst. According to the deconvolution results, the Ti 2*p* spectrum of all catalysts is dominated by species with a binding energy (BE) of the Ti $2p_{3/2}$ photoelectrons of 458.7 eV related to the Ti^{4+} oxidation state. Besides, a small contribution (≅3–4%) of reduced species Ti^{3+}, which appears at a BE of < 2.5 eV below the Ti^{4+} peak, is detected. The asymmetrical O 1*s* spectra can be deconvoluted into three components. The major component at BE ≅530 eV is obviously related to O^{2-} species, while two minor components at ≅531.2 and ≅532.2 eV may be attributed to the presence of the surface hydroxyl groups OH^- on TiO_2 support

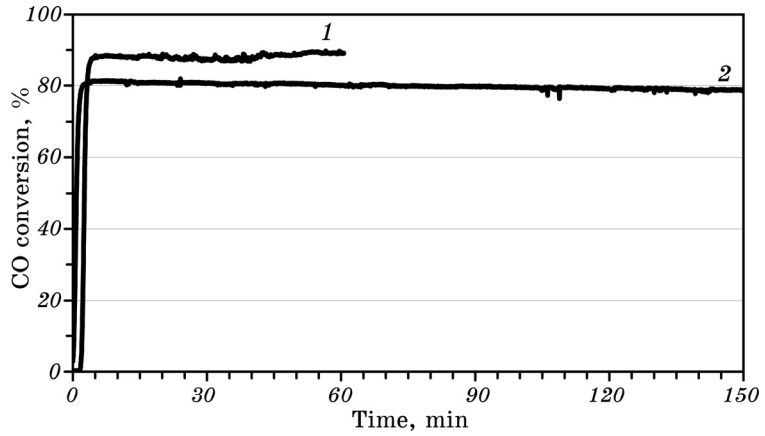

Fig. 1. CO-to-CO_2 conversion at room temperature as a function of reaction time over Au/TiO_2 catalysts prepared by the deposition–precipitation routes DP1 (curve *1*) and DP2 (curve *2*). See text for details of preparation.

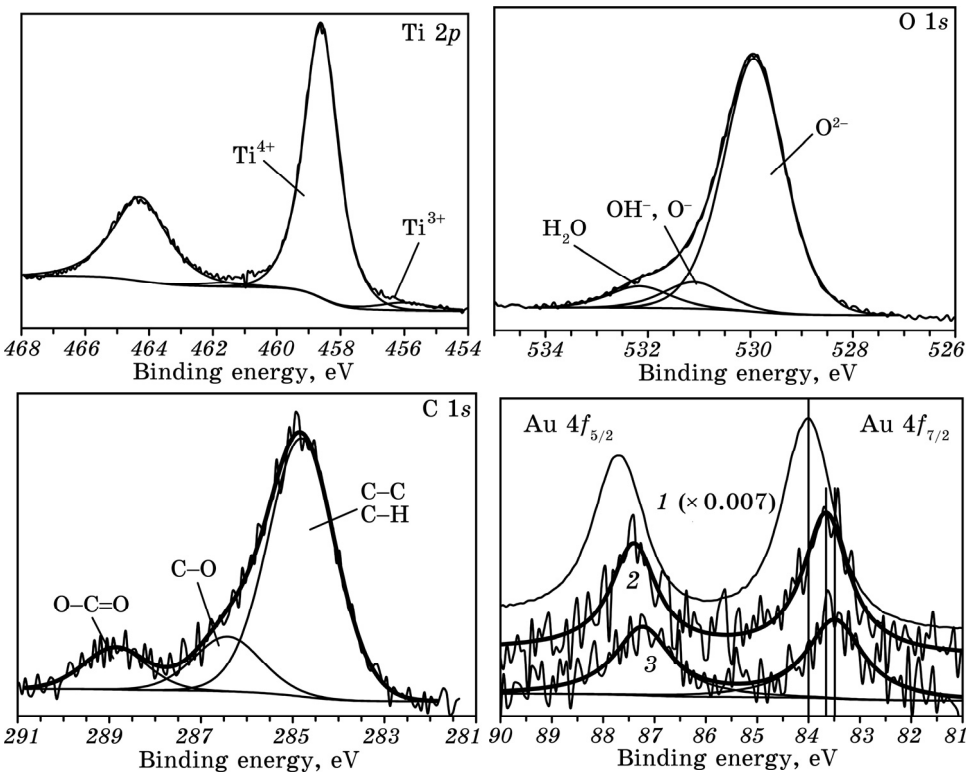

Fig. 2. Ti 2*p*, O 1*s*, C 1*s* and Au 4*f* XPS core level spectra for an Au/TiO_2 catalyst. The presented Au 4*f* spectra correspond to pure Au foil (*1*), fresh (*2*) and used Au/TiO_2 catalyst (*3*). The binding energy scale is corrected for surface charging effect. Chemical species derived from deconvolution of the spectra are indicated.

(and/or subsurface low-coordinated oxygen ions O^-) and adsorbed water molecules, respectively. Interpretation of the O 1*s* peak structure for Au/TiO_2 catalysts and TiO_2 was recently discussed in detail elsewhere [12]. The C 1*s* spectrum of the Au/TiO_2 catalysts is dominated by C–H/C–C species at BE = 284.8 eV resulting from contamination of the surface by hydrocarbons (adventitious carbon). The minor components at 286.4 eV and 288.9 eV correspond to C–O and O=C–O species, respectively [14]. The position of the Ti $2p_{3/2}$, O 1*s* and C 1*s* peaks did not change after using the catalysts in the reaction of CO oxidation.

Fitting the Au 4*f* spectra of the Au/TiO_2 catalysts shows gold nanoparticles to be exclusively in a single metallic state. As can be seen in Fig. 2, the Au 4*f* spectrum of fresh catalyst is shifted with respect to the spectrum of Au foil toward lower binding energies. In fresh DP1 and DP2 catalysts, the Au $4f_{7/2}$ BE corrected for charging effect turned

out to be lower than that in bulk Au by 0.36 ± 0.02 eV and 0.31 ± 0.02 eV, respectively, implying that Au clusters are electronically different from bulk Au. A similar negative shift of the Au 4*f* line was also observed for World Gold Council standard Au/TiO_2 catalyst and was discussed in detail in the previous work [12]. The negative shift of the Au 4*f* BE indicates a charge transfer from TiO_2 to Au atoms making them somewhat negatively charged [15]. The strong interaction of the interfacial Au atoms with reduced Ti^{3+} species of the support, yielding $Au^{\delta-}$ electronic state of gold atoms, is considered [16] to be crucial for activation of O_2. According to *ab initio* calculations, the extra negative charge on the anionic Au clusters as compared to the neutral clusters can enhance not only O_2 adsorption but also the strength of coadsorption of CO and O_2, which leads to a lower reaction barrier in the oxidation step and, consequently, to a higher catalytic activity [17].

The reaction of CO oxidation carried out over Au/TiO_2 catalysts has caused significant changes in the electronic state of Au nanoparticles, both after short (1 h, DP1) and long (2.5 h, DP2) time on stream. Indeed, as can be seen from Fig. 2 and 3, *a*, after catalytic reaction a further decrease of the Au 4*f* BE in the used catalyst occurred as compared with the fresh one, with the total negative shift with respect to the bulk Au amounting to 0.45 ± 0.05 eV for DP1 and 0.41 ± 0.03 eV for DP2. This observation is in agreement with other works [6, 7, 18] reporting a similar shift of the Au 4*f* spectrum toward lower binding energies for Au/TiO_2 catalysts used in the CO oxidation reaction. The additional negative shift of the Au 4*f* line in the used catalyst may result

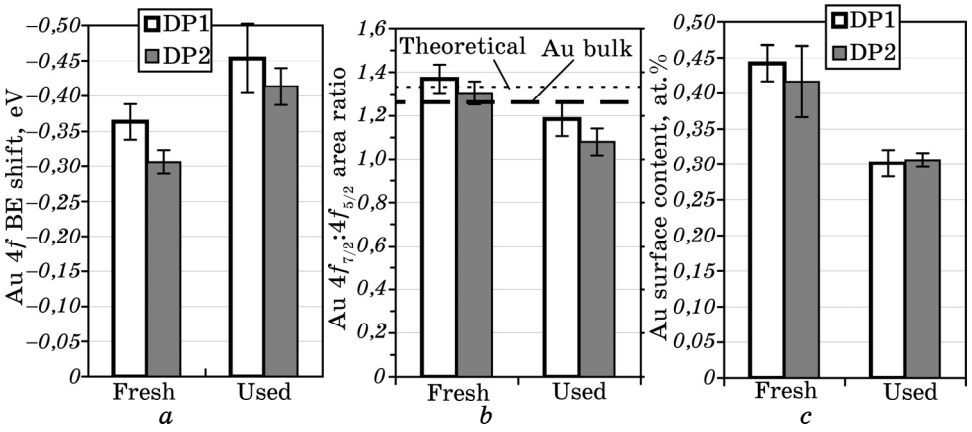

Fig. 3. The shift of the Au $4f_{7/2}$ binding energy in Au/TiO_2 catalyst with respect to that in bulk Au (*a*), the ratio of intensities of the Au $4f_{7/2}$ and $4f_{5/2}$ spin orbit peaks (*b*) and the Au surface atomic concentration (*c*) derived from XP spectra of DP1 and DP2 catalysts in the fresh state and after using in the reaction of CO oxidation.

from reaction-induced enhancement of charge transfer to the gold atoms (or stronger interaction of Au nanoparticles with the support) and/or interaction of CO with Au nanoparticles giving rise to formation of stable $Au^{\delta-}$–CO species [19].

Other parameters of the Au 4*f* spectrum also suffered transformation. Due to spin-orbit coupling effects, the 4*f* photoemission from Au is in fact split between two peaks with different BE, Au $4f_{7/2}$ and Au $4f_{5/2}$, which correspond to final states with total angular momentum $J_+ = L + S = 7/2$ and $J_- = L - S = 5/2$, respectively. The relative intensities of the two peaks reflect the degeneracy of the final spin states and are described by the ratio $(2J_+ + 1)/(2J_- + 1)$. In the fresh Au/TiO_2 catalysts, the Au $4f_{7/2}$-to-$4f_{5/2}$ area ratio for the two spin-orbit peaks was close to a theoretical value of 4/3 and was higher than that measured for the bulk Au (1.26 ± 0.02) (Fig. 3, *b*). After catalytic reaction the $4f_{7/2}$:$4f_{5/2}$ peak area ratio noticeably decreased (by 13.5% for DP1 and 17.2% for DP2). This redistribution of intensity of the spin orbit peaks in the used catalyst observed for the first time indicates the change in the probability of transition to a degenerate spin state during photoionization, which may be caused by reaction-induced modification of the structural and electronic state of Au atoms.

In the fresh Au/TiO_2 catalysts, the surface gold content evaluated from XPS data was 0.42–0.44 at.%. Small variations in the concentration of Au on the surface of DP1 and DP2 at the same Au loading may result from different dispersion of supported Au nanoparticles. After catalytic reaction the surface Au concentration in the catalysts decreased to 0.3 at.%, *i.e.* by about 30% as compared with the fresh sample (Fig. 3, *c*). Respectively, the Au/Ti atomic ratio, which characterizes dispersion of Au nanoparticles, decreased after catalytic test from 0.013 to 0.009. Such a noticeable 'apparent' decrease in the Au content, which was also observed in works [6, 10], indicates a decrease in the Au coverage associated with agglomeration and 3*D*-growth of Au nanoparticles occurring effectively during both short and long reaction time. Note, however, that this reaction-induced agglomeration process, which manifested itself in a 30% decrease of the Au coverage, did not lead to an appreciable deactivation of the catalysts (Fig. 1).

The reaction-induced agglomeration, or sintering, of Au nanoparticles was observed in a number of works. According to high-resolution TEM measurements, the reaction of CO oxidation over the Au/TiO_2 catalyst at 30°C for ≅33 h [9] or at 200°C for ≅6 h [18] caused the increase in the average gold particle size by about 50% and 76%, respectively. In Au/Al_2O_3 catalyst, after 7 h of CO oxidation at room temperature, the mean width of the gold particles increased from 2.3 to 3.2 nm [8], mainly due to aggregation of smaller Au nanoparticles. Recent *in situ* studies using scanning tunnel microscopy [20] revealed that sintering of Au nanoparticles supported on TiO_2(110) began im-

mediately upon the introduction of a $CO/O_2 = 1/1$ gas mixture and proceeded via Ostwald ripening. After 2 h of CO oxidation at room temperature, the number density of the Au particles decreased by ≅57% and then decreased slowly thereafter. It was established that the activation energy of sintering for Au particles correlates with the activation energy of CO oxidation and is consistent with a reaction-induced mechanism. Thus, we can conclude that the large amount of energy released during the exothermic CO oxidation reaction [8] occurring on the surface of the Au/TiO_2 catalyst could be enough to promote changes in the morphology and electronic structure of gold nanoparticles and local alterations in the support after several hours on stream.

The CO oxidation-induced decrease in the Au surface coverage observed with XPS correlates with an appreciable decrease in the surface content of Na and K impurities detected by SIMS (cf. Figs. 3, *c* and 4, *a*), which, due to its high sensitivity, allows detection of alkali elements at a very low level. This may be related to the interaction and association of alkali atoms with Au nanoparticles forming active centres $Au^{\delta-}Na^+$, $Au^{\delta-}K^+$. Note that the relative emission of $NaTiO^+$ and $KTiO^+$ secondary ions characterizing interaction of alkali atoms with the TiO_2 support somewhat increased after reaction (Fig. 4, *b*) in accordance with a decrease in the Au particle surface coverage.

Figure 5 compares the atomic concentration of different oxygen species, O^{2-}, OH^- and H_2O, derived from the O 1*s* spectra (Fig. 2) on the surface of the fresh and used DP1 and DP2 catalysts. In DP1, the content of the lattice oxygen O^{2-} in the support slightly increased after reaction (by ≅2.1%), whereas in DP2 it decreased by ≅3.2% (Fig. 5, *a*). Accordingly, the O^{2-}/Ti atomic ratio changed from 2.03 ± 0.08 to

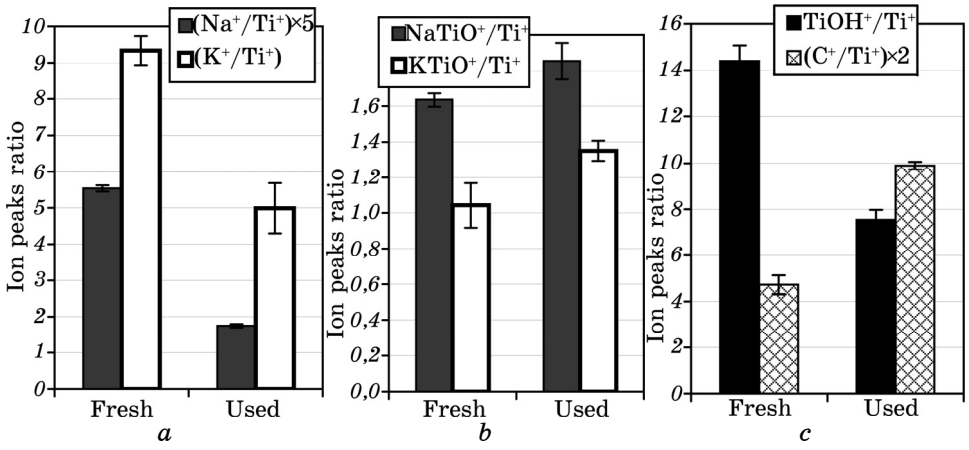

Fig. 4. The emission of Na^+, K^+ (*a*), $NaTiO^+$, $KTiO^+$ (*b*), $TiOH^+$ and C^+ secondary ions normalized by emission of Ti^+ ions from fresh and used DP2 catalyst.

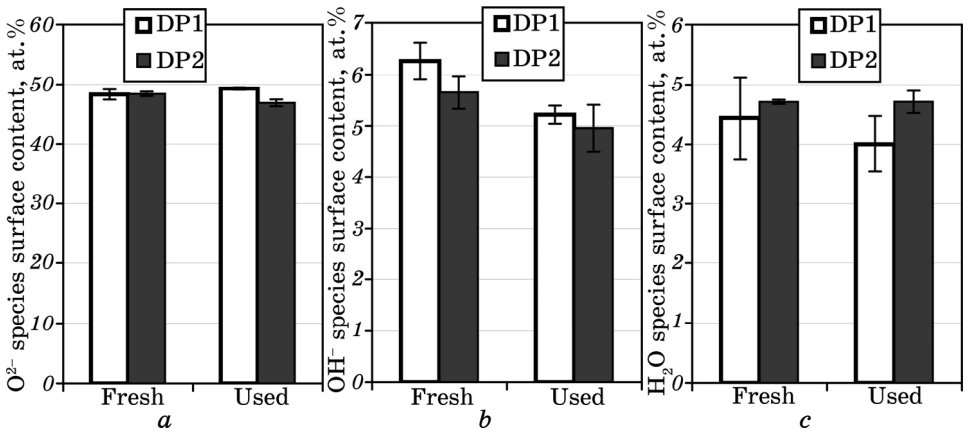

Fig. 5. The concentration of O^{2-} (*a*), OH^- (*b*) and H_2O species on the surface of fresh and used DP1 and DP2 Au/TiO_2 catalysts derived from the O 1*s* XP spectra.

2.11 ± 0.05 in DP1 and from 2.08 ± 0.02 to 2.04 ± 0.03 in DP2. Consistent alterations occurred also in the Ti 2*p* spectra (Fig. 2). In DP1, the fraction of reduced Ti^{3+} species decreased as a result of the catalytic reaction from 4.4 to 3.8%, whereas in DP2 the Ti^{3+} fraction increased from 4.5 to 5.3%. Such variations of the O^{2-}/Ti atomic ratio and the Ti^{3+} fraction in DP1 and DP2 imply that, depending on duration of the test, the catalytic reaction can cause either some additional oxidation of the support or, on the contrary, some reduction of TiO_2 due to participation of the lattice oxygen in the reaction of CO oxidation, *i.e.* the processes of reduction-oxidation of the support during the course of reaction appear to be alternating.

Emission of characteristic molecular secondary ions such as $TiOH^+$, $TiOH_2^+$, TiO_2H^+, $Ti_2OH_3^+$, OH^+ and H_2O^+ observed by SIMS and occurrence of the O 1*s* components at $\cong 531$ eV and $\cong 532$ eV in XPS (Fig. 2) for the Au/TiO_2 catalyst indicate the presence of hydroxyl groups and adsorbed water on the support surface. The hydroxylation and hydration of the catalyst surface may originate from using the oxalic acid dihydrate $C_2O_2(OH)_2 \cdot 2H_2O$ for precipitation of titanium oxalate or/and from adsorption of water and formation of hydroxyl groups on the surface of the calcined catalysts in atmosphere.

As can be seen in Figure 5, *b*, the content of OH^- groups in fresh catalyst DP1 is larger than in DP2. This is consistent with a smaller O^{2-}/Ti^{4+} atomic ratio in DP1 as mentioned above and may indicate a partial substitution of oxygen atoms in the lattice of TiO_2 by hydroxyl groups. The higher level of the initial surface hydroxylation in fresh DP1 may be favourable for attaining a higher catalytic activity as compared with DP2 (Fig. 1). Indeed, as has recently been shown [21],

the activity of supported Au catalysts in CO oxidation increases with increasing the extent of support hydroxylation. The important role of surface hydroxyls in the enhancement of activity of the Au/TiO_2 catalyst was assigned [22] to a significant charge transfer at the interface of the Au nanoparticle and TiO_2 that resulted in reducing the CO oxidation reaction barrier. The hydroxyl group adsorbed on the support and bonded to an Au cation or to a highly coordinatively unsaturated metallic Au atom at the periphery of Au nanoparticle was also considered [1, 23, 24] to be a part of the active site involved in CO oxidation.

The surface content of the hydroxyl-related component OH^- in DP1 and DP2 catalysts derived from the O 1*s* spectra decreased after reaction by about 17% and 12%, respectively (Fig. 5, *b*). The XPS data are supported by SIMS measurements, which display a noticeable decrease in the emission of OH^+ and $TiOH^+$ ions after using the catalyst in the reaction (Fig. 4, *c*). These results are in accordance with *in situ* Diffuse Reflectance Infrared Fourier Transform Spectroscopy (DRIFTS) observations of the loss of OH groups from the support during the reaction of CO oxidation over Au/TiO_2 catalyst [18, 25]. As distinct from the hydroxyls, the amount of adsorbed water estimated from the O 1*s* spectra did not change much after the reaction (Fig. 5, *c*).

The loss of hydroxyl groups in the used catalysts is consistent with a mechanism [23, 24], which is based on the active site model mentioned above. According to this mechanism, CO adsorbed on metallic Au is inserted into an Au–OH bond to form a hydroxycarbonyl ($-CO + OH \rightarrow \rightarrow OCOH^-$). The hydroxycarbonyl is oxidized to a bicarbonate HCO_3^-, which is then decomposed into Au–OH and CO_2. In addition to decomposing to CO_2, the bicarbonate intermediate also reacts by a parallel pathway of deprotonation with substrate hydroxyl to form a carbonate ($HCO_3^- + OH \rightarrow CO_3^{2-} + H_2O$). The carbonate on the catalyst surface can also be formed by the reaction of hydroxycarbonyl with surface hydroxyl groups ($O\underline{C}OH^- + OH \rightarrow CO_3^{2-} + H_2O$) [19], whereas the reaction of adsorbed CO with bridging hydroxyl groups can fuel formation of relatively inactive formate species $HCO\underline{O}^-$ [18]. Thus, the hydroxyls participate in the reaction and are consumed accordingly to produce formates/carbonates, *i.e.* the support is depleted of OH groups during the reaction. The formation of various carbon-containing species on the catalyst surface was evidenced by both XPS and SIMS measurements as described below.

In fresh catalysts DP1 and DP2, the respective surface concentrations of carbon-containing species C–C, C–O and O–C=O derived from C 1*s* spectra (Fig. 2) were about the same, and after the reaction of CO oxidation, they all increased. Accordingly, an increase in the total surface carbon content after using the catalysts in the reaction was detected in both XPS (as represented by the full C 1*s* peak area in Fig. 6) and SIMS (as represented by the C^+/Ti^+ ion peaks ratio in Fig. 4, *c*). The

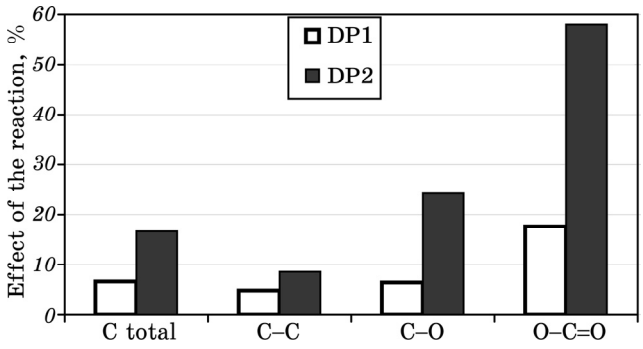

Fig. 6. The relative change of the surface concentration of various carbon-containing species caused by the reaction of CO oxidation, $(C_{used} - C_{fresh})/C_{fresh}$, derived from the C 1*s* XP spectra of DP1 and DP2 catalysts.

relative change of the surface concentration of carbon-containing species induced by the CO oxidation, $(C_{used} - C_{fresh})/C_{fresh}$, or effect of the reaction, is plotted in Fig. 6 for DP1 and DP2. As can be seen, the reaction-induced additional formation of various carbon species in both catalysts is enhanced in the series C–C < C–O < O–C=O, with the largest augmentation being observed for the carboxylate group O–C=O (by ≅18% for DP1 and ≅58% for DP2). It is noteworthy that with increasing time on stream the concentrations of all the carbon species and the total carbon content appreciably increase (cf. reaction effects for DP1 and DP2 in Fig. 6).

Furthermore, emission of molecular ions TiC^+, $TiCO^+$, $TiCOH^+$, $TiCO_2^+$, $TiCO_2H^+$, $TiCO_3^+$, and $TiCO_3H^+$ observed from fresh catalysts indicates the presence already in the initial state of various functional groups such as carbonyl (–C=O), hydroxy (–C–OH) or formyl (H–C=O), carboxylate (O–C=O), hydroxycarbonyl (O=C–OH) or formate (O–CH=O), carbonate (OO–C=O), and bicarbonate (OO–C–OH). Apparently, these species were formed on the support surface as a result of interaction of atmospheric CO_2 and moisture with TiO_2 [19, 26] which is corroborated by nearly the same intensity of emission of these ions from the fresh Au/TiO_2 catalyst and pure TiO_2 (Fig. 7). Using the catalyst in the reaction of CO oxidation gave rise to a noticeable increase in the ion emission of all the carbon-containing species (Fig. 7) that evidences their accumulation on the support surface. The enhanced emission of $TiCO_2^+$ and $TiCO_2H^+$ ions from the used catalyst (Fig. 7) may indicate a higher population of carboxylate and hydroxycarbonyl/formate moieties on the catalyst surface as compared to other species. On the other hand, the largest relative change of the emission after the catalytic reaction was observed for $TiCO_3^+$ and $TiCO_3H^+$ ions (≅98% and ≅136%, respectively), which implies the preferential formation of carbonate and bicarbonate groups. These results are consistent with

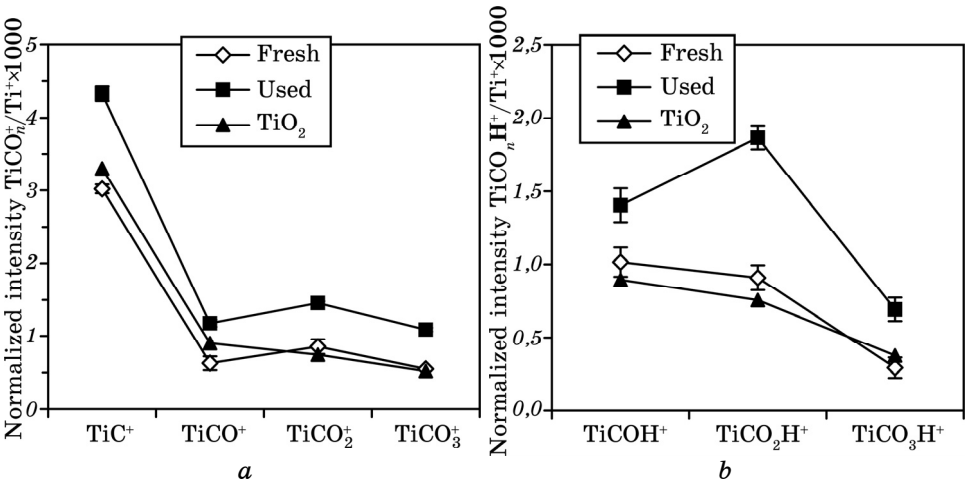

Fig. 7. The emission of TiC^+, $TiCO^+$, $TiCO_2^+$, $TiCO_3^+$ (*a*) and $TiCOH^+$, $TiCO_2H^+$, $TiCO_3H^+$ (*b*) secondary ions normalized by emission of Ti^+ ions from fresh and used Au/TiO_2 DP2 catalyst and from TiO_2.

XPS data (Fig. 6) and agree with DRIFTS measurements showing formation and build-up of carbonates, carboxylates, hydroxycarbonyls/formates, and bicarbonates on Au/TiO_2 during CO oxidation [6, 9, 18, 19, 25]. The point whether the carbonates reside on the gold [19], on the support [9, 18, 27], on the Au–TiO_2 border [6], or on both the Au and the support [28] is still in debate. Our SIMS data demonstrating an intense emission of molecular ions $TiCO_2^+$, $TiCO_2H^+$, $TiCO_3^+$, and $TiCO_3H^+$ from the used catalyst suggest that these carbonate-like species are not intermediates in the reaction mechanism but strongly bound to the catalyst and most likely reside on the titania support.

The loss of activity with time on stream is a crucial factor that could hamper the industrial development of gold-based catalysts. Deactivation of the catalyst was suggested to occur due to reduction of oxidized gold species (which were claimed to be the most active sites for CO oxidation) to metallic gold [3, 4], sintering of Au nanoparticles (irreversible) [6, 15, 18], dehydroxylation of the support during the reaction (assuming that OH groups were involved in the oxidation pathway) [23, 24], and accumulation of carbonate-like species (carbonate CO_3^{2-}, formate HCO_2^- and carboxylate O–C=O groups) at the active sites [6, 9, 19, 25, 27, 28]. In our work, some sintering, dehydroxylation and build-up of surface carbonate-like species occurred in the catalyst (DP1) already after 1 h on stream, although no deactivation was observed (Fig. 1, curve *1*). On the other hand, the catalyst DP2, which is characterized by a significantly larger extent of the surface carbonization after 2.5 h on stream (Fig. 6) at nearly the same levels of sintering

(Fig. 3, *c*) and dehydroxylation (Fig. 5, *b*), did demonstrate some decline of activity (Fig. 1). This indicates the decisive role in deactivation of carbonate-like species, which gradually accumulate during the reaction, covering the surface and acting as catalyst poison. A partial regeneration of activity may occur via reaction of carbonates with adsorbed H_2O and/or of formates with activated oxygen to form thermally less stable bicarbonates with their subsequent decomposition ($-CO_3 + + H_2O \rightarrow -CO_3H + OH$, $HCO_2^- + O^* \rightarrow -CO_3H$, $-CO_3H \rightarrow CO_2 + OH$) [24, 25].

4. CONCLUSIONS

Using the Au/TiO_2 catalyst in the reaction of CO oxidation at room temperature for 1–2.5 h on stream gives rise to a number of changes in the morphological and electronic state of Au nanoparticles and chemical composition of the support. As has been observed, the catalytic reaction causes some agglomeration, or sintering, of Au nanoparticles and enhances electron transfer to the gold atoms making them more negatively charged. The reaction-induced modification of the structural and electronic state of Au atoms results in the redistribution of intensity of the Au 4*f* spin orbit peaks in the used catalyst. The reaction of CO oxidation is accompanied by the loss of hydroxyl groups and the noticeable accumulation of various carbon-containing species on the support surface with the preferential formation of carbonate and bicarbonate groups. These moieties appear to block the active sites and thus play a key role in the gradual deactivation of the catalyst.

A partial financial support of this work from the National Academy of Sciences of Ukraine in the framework of the Fundamental Research Program 'Fundamental Problems of Nanostructural Systems, Nanomaterials, Nanotechnologies 2010–2014' is greatly acknowledged.

REFERENCES

1. J. C. Bond and D. T. Thompson, *Gold Bull.*, **33**: 41 (2000).
2. E. A. Willneff, S. Braun, D. Rosenthal, H. Bluhm, M. Hävecker, E. Kleimenov, A. Knop-Gericke, R. Schlögl, and S. L. M. Schroeder, *J. Am. Chem. Soc.*, **128**: 12052 (2006).
3. E. D. Park and J. S. Lee, *J. Catal.*, **186**: 1 (1999).
4. A. M. Visco, F. Neri, G. Neri, A. Donato, C. Milone, and S. Galvagno, *Phys. Chem. Chem. Phys.*, **1**: 2869 (1999).
5. A. M. Venezia, G. Pantaleo, A. Longo, G. Di Carlo, M. P. Casaletto, F. L. Liotta, and G. Deganello, *J. Phys. Chem. B*, **109**: 2821 (2005).
6. P. Konova, A. Naydenov, Cv. Venkov, D. Mehandjiev, D. Andreeva, and T. Tabakova, *J. Mol. Catal. A: Chem.*, **213**: 235 (2004).
7. S. Arrii, F. Morfin, A. J. Renouprez, and J. L. Rousset, *J. Am. Chem. Soc.*, **126**: 1199 (2004).

8. G. M. Veith, A. R. Lupini, S. J. Pennycook, G. W. Ownby, and N. J. Dudney, *J. Catal.*, **231**: 151 (2005).
9. Y. Denkwitz, Z. Zhao, U. Hörmann, U. Kaiser, V. Plzak, and R. J. Behm, *J. Catal.*, **251**: 363 (2007).
10. P. Konova, A. Naydenov, T. Tabakova, and D. Mehandjiev, *Catal. Commun.*, **5**: 537 (2004).
11. L.-C. Wang, Q. Liu, X.-S. Huang, Y.-M. Liu, Y. Cao, and K.-N. Fan, *Appl. Catal. B*, **88**: 204 (2009).
12. N. Kruse and S. P. Chenakin, *Appl. Catal. A: Gen.*, **391**: 367 (2011).
13. *Handbook of X-Ray Photoelectron Spectroscopy* (Eds. C. D. Wagner, W. M. Riggs, L. E. Davis, J. F. Moulder, and G. E. Muilenberg) (Eden Prairie: Perkin-Elmer Corp.: 1979).
14. G. P. Lypez, D. G. Castner, and B. D. Ratner, *Surf. Interface Anal.*, **17**: 267 (1991).
15. D. W. Goodman, *Catal. Lett.*, **99**: 1 (2005).
16. A. Vijay, G. Mills, and H. Metiu, *J. Chem. Phys.*, **118**: 6536 (2003).
17. Y. Gao, N. Shao, Y. Pei, Z. Chen, and X. C. Zeng, *ACS Nano*, **5**: 7818 (2011).
18. K. Y. Ho and K. L. Yeung, *J. Catal.*, **242**: 131 (2006).
19. M. C. Raphulu, J. McPherson, E. van der Lingen, J. A. Anderson, and M. S. Scurrell, *Gold Bull.*, **43**: 334 (2010).
20. F. Yang, M. S. Chen, and D. W. Goodman, *J. Phys. Chem. C*, **113**: 254 (2009).
21. C. J. Karwacki, P. Ganesh, P. R. C. Kent, W. O. Gordon, G. W. Peterson, J. J. Niu, and Y. Gogotsi, *J. Mater. Chem. A*, **1**: 6051 (2013).
22. P. Ganesh, P. R. C. Kent, and G. M. Veith, *J. Phys. Chem. Lett.*, **2**: 2918 (2011).
23. C. K. Costello, M. C. Kung, H.-S. Oh, Y. Wang, and H. H. Kung, *Appl. Catal. A: Gen.*, **232**: 159 (2002).
24. M. C. Kung, R. J. Davis, and H. H. Kung, *J. Phys. Chem. C*, **111**: 11767 (2007).
25. B. Schumacher, Y. Denkwitz, V. Plzak, M. Kinne, and R. J. Behm, *J. Catal.*, **224**: 449 (2004).
26. J. C. Clark, S. Dai, and S. H. Overbury, *Catal. Today*, **126**: 135 (2007).
27. J. Saavedra, C. Powell, B. Panthi, C. J. Pursell, and B. D. Chandler, *J. Catal.*, **307**: 37 (2013).
28. B. Schumacher, V. Plzak, M. Kinne, and R. J. Behm, *Catal. Lett.*, **89**: 109 (2003).